

## CONTOURED 3D PRINTING OF FIBER REINFORCED POLYMERS

L. Y. L. Tse\*, S. Kapila†, and K. Barton\*

\*Department of Mechanical Engineering, University of Michigan, Ann Arbor, MI 48109

†Department of Orofacial Science, University of California, San Francisco, CA 94143

### Abstract

*Additive manufacturing (AM) is a cost effective approach for small-scale production, providing higher design flexibility and less material waste than traditional manufacturing techniques. Polymers constitute one of the most popular AM materials, yielding lightweight but inherently weak components that cannot hold up against high tension and bending stresses. A need for improved tensile strength has driven a recent interest in AM of fiber reinforced polymers (FRPs). AM-FRPs reinforced with short fibers have demonstrated increased mechanical strength, but with limited design and structural flexibility. AM-FRPs reinforced with continuous fibers provide structural reinforcement within plane; as such, the fibers cannot be extruded along a contoured profile, significantly minimizing the application space for these AM-FRP devices. In this article, we address this current gap through the development of a new FRP additive manufacturing process that is capable of continuous fiber deposition along contoured trajectories. Experimental demonstrations validate the proposed process.*

### Introduction

Additive Manufacturing (AM) is a relatively new manufacturing concept that is driving a new paradigm in advanced manufacturing [1-3]. By continuously attaching small quantities of material at precisely controlled locations, additive manufacturing allows the user to fabricate intricate geometries using polymer, metal, ceramic, or biological tissues and materials. Unlike many traditional manufacturing techniques, AM processes do not require templates, molds or masks; thus, AM leverages the distribution of material at specific locations to achieve unique device designs with time and cost savings for small to medium-scale production. Additionally, AM has the unique ability to fabricate interlocking geometries, features embedded within a shell structure, and heterogeneously printed materials within a single layer or design, leading to new designs and functionalities [4].

Polymer inks were among the first materials utilized in AM for prototyping functional devices [4], and have remained the most commonly used material to date. Recent advancements in material properties and AM processing capabilities have led to new AM materials for a wider range of applications. Flexible polymers such as polycaprolactone (PCL) and Nylon have recently been demonstrated for 3D printing [5,6]; these materials result in lightweight and geometrically customized parts, such as prosthetic limbs and robotic frames. Despite the advantages for customized prosthetics and robotic systems [7,8], the tensile strength of these materials is significantly lower than standard metal materials or that required for optimal functionality [9].

Current advancements in polymer materials have resulted in fibers (specifically carbon fibers) being combined with a polymer into a single material to generate fiber-reinforced polymers (FRPs or CFRPs for carbon fiber reinforced polymers). The use of fibers embedded within the

polymer layers increases the strength-to-weight ratio and improves resistance against tension versus standard polymers (see <https://markforged.com/materials/>). Current FRP parts are fabricated through traditional approaches that involve stacking up layers of fibers and polymer on a mold or template, and applying heat or chemical curing to adhere the different layers together. This method has resulted in parts with significant increases in strength along the direction of the fibers. One common use of FRPs is towards the development of shell-structures for automotive applications. Despite the advantages in structural strength, this fabrication process is time consuming, expensive, and inflexible to design changes; a new mold is needed for each design change.

To address these fabrication limitations with FRP, AM of FRPs has garnered recent significant interest. Two common techniques for AM of FRP include: 1) printing of a mixture containing polymer and short fiber fragments using a standard Fused Deposition Modeling (FDM) technique [10], and 2) repeatedly printing alternative layers of polymer and continuous fiber with the FDM approach (Markforged printers). A core disadvantage of the first approach stems from the weak physical bonding between the short fibers. Short fibers do not produce significant reinforcements within the material as they lack a structured orientation and continuity against stress and strain forces. In contrast to short FRPs, continuous FRPs provide a large resistance force against tension and large bending strains, particularly along the optimum orientation due to the aligned positioning of the fibers. Despite the potential advantages of this approach, continuous FRP printing has yet to be translated into a commercially viable additive manufacturing technique.

Markforged has developed the first and currently only commercialized continuous FRP 3D printers. Structurally, Markforged printers are very close to that of regular FDM machines. The system prints a layer of polymer using a traditional FDM approach in which the polymer undergoes a phase transition (thermally melted) prior to being deposited onto the substrate surface. Following the polymer deposition, strands of continuous fiber are placed onto the melted polymer surface in rastered or looped patterns. A significant disadvantage of the current printer design is the restriction to 2D printing of fiber layers due to (1) the two-step layering process that requires at least one layer of polymer to be deposited prior to the fiber strands, and (2) bulky and rigid printheads that prohibit contour following. ***As such, true 3D deposition of contoured fiber reinforced polymers has yet to be realized, prohibiting FRP shell-structures from being 3D printed.***

To address this important technical gap in 3D printing of FRPs, the authors have developed a new 3D printing methodology that enables 3D contoured deposition of FRP. This manuscript presents a 3D printing system that enables the placement of continuous FRP filaments onto contoured surfaces (e.g. XYZ fiber placement in real-time), thereby allowing the user to create shell-structures similar to the structures fabricated with traditional manufacturing approaches. One important advantage of 3D printing these structures is the ability to customize the designs on a case-by-case basis.

The manuscript is arranged as follows. Section II provides some background information on FDM and the application needs for additive manufacturing of FRPs. Section III introduces the design and development of a critical element in the printing process known as the co-axial fiber, which is a polymer-coated fiber that provides rigidity and adherence within the combined structure. Section IV provides additional details of the printhead including the unique features in the design that have led to the development of true 3D printing of FRPs. A demonstration of the

capability of the printhead is presented in section V. A discussion of design challenges, printing process limitations, and future development directions is given in section VI. Section VII contains concluding remarks.

## **Background**

### **A. Fused Deposition Modeling (FDM)**

Conventional FDM follows the additive paradigm of depositing material in successive layers in order to produce a 3-Dimensional (3D) part. Contrary to powder or ink-based deposition processes, FDM extrudes flattened lines of molten material to form layers that rapidly solidify upon extrusion from the nozzle. Commonly available FDM materials, such as Acrylonitrile-Butadiene-Styrene (ABS) and polylactic acid (PLA), are thermoplastics; that is they become molten when heat is applied to them and cool rapidly in air after the heating source is removed. Moreover, their molten forms are viscoelastic fluids that enable these materials to sustain their own weight and shape upon release from the nozzle, resulting in printed filaments with ~1:1 aspect (height-to-width) ratio. By overlapping 2D patterns printed with filaments of ~1:1 aspect ratio, the FDM process can create very complicated 3D structures that are challenging to produce with traditional manufacturing techniques such as lithography or micromachining.

As described previously, existing FRP printers apply a conventional FDM approach with either continuous or short fibers. The short FRPs are not as flexible and lack an optimum loading orientation, while continuous FRP can only align fibers in planar directions. Importantly, the ability to deposit contoured shapes cannot currently be achieved using the conventional FDM printers.

### **B. Applications for FRP**

FRPs that have optimal shape and properties have a multitude of potential applications in the automotive, aerospace and medical fields. To meet the rising regulations for environment protection [11] and safety standards [12, 13], there is a growing demand for FRPs that reduce the weight of automobiles, while simultaneously making their structures more effective in shock energy absorption [14]. Additionally, as more alternative fuels are being adopted in the automotive industry [16], there is an increasing need for materials that withstand the unique conditions created by these fuels within the power-train. These developments have led to an increasing demand for new manufacturing technologies that enable the fabrication of FRP-based power-trains, battery casings and thermal management systems that are capable of withstanding the harsh environments introduced by these different fuels.

In the medical field, assistive devices, in particular ankle-foot orthoses (AFOs), artificial limbs and increasingly robotics, are custom-made medical devices that correct for a variety of acquired or congenital defects in patients. The current, widely-adopted, manufacturing approach for fabricating AFOs is a plaster casting method that requires multiple fittings, a costly and time-intensive fabrication process, and results in repeat visits for adjustments and additional modifications [17]. Additive manufacturing of FRPs provides an alternative fabrication approach that has the potential to decrease production times, lower waste and energy consumption, decrease costs, and improve AFO customization and user performance [18-20].

In the following sections, we will discuss the materials, features and design challenges of our FRP printing system.

### Co-axial Fiber

An important difference between existing FRP 3D printers and the system described herein resides in the use of a spool of polymer coated fiber filament known as the co-axial fiber, as opposed to adhering fiber threads onto a polymer foundation used in currently available FRP printers. The spool of material is fed through a nozzle, while simultaneously melting the outer coating and adhering the filament fibers to previously printed material. This approach provides three important advantages over existing technology and methods: (1) the more rigid structure of the co-axial fiber enables the printer to deposit material along contoured surfaces and achieve overhanging features, which have not yet been realized with conventional FRP printing; (2) the one-step approach provides faster fabrication with less material waste; (3) the co-axial fiber provides important structural advantages such as the reduction of buckling during fabrication as compared to fiber threads currently in use.

#### A. Raw Materials

The raw materials in this process consist of the fiber and polymer materials that are used to make-up the FRP strands. Printing demonstrations in this manuscript utilize carbon fibers due to the ubiquitous use of this material in practice; however, potential fiber materials can be expanded to include Kevlar, glass fibers, metal wires, and medical suture materials.

The polymer base used in the manuscript consists of Polycaprolactone (PCL). Additional polymer options may include nylon and ABS, among others. As discussed previously, FDM compatible polymers exhibit a viscoelastic molten form and rapid solidification property; thus allowing the polymer to maintain a ~1:1 aspect ratio during deposition. The approach presented here utilizes co-axial fibers that maintain the 1:1 aspect ratio through the fiber thread rather than the polymer. Therefore, candidate polymers do not have to exhibit a viscoelastic molten form or rapid solidification property; polymer compatibility with this printing system is significantly more diverse than conventional FDM systems.

#### B. Co-axial Fiber Fabrication

The co-axial filament is fabricated using the set-up depicted in fig. 1. The setup consists of a heat sink, a heating element, a temperature controller, a syringe barrel that holds a reservoir of molten polymer (PCL), a frame structure, a motor and a spool core to collect the co-axial fiber filament.

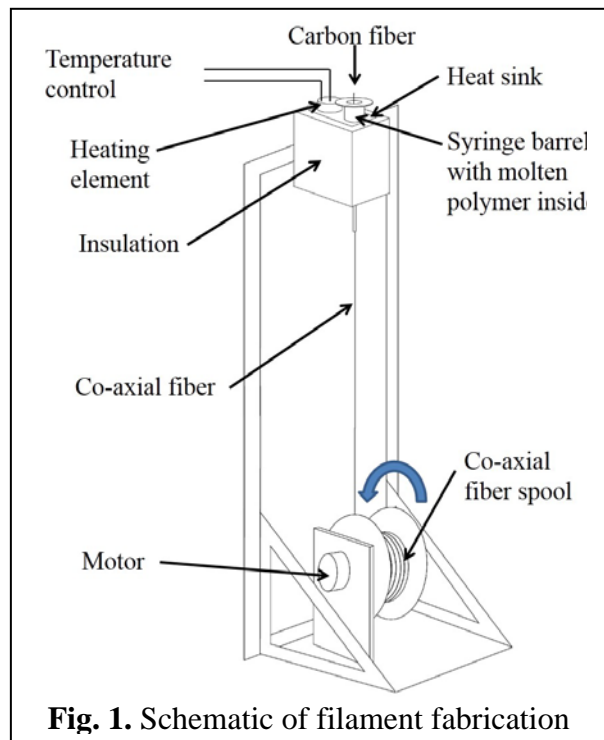


**Fig. 1.** Schematic of filament fabrication

The coating process requires the carbon fiber to be continuously pulled through the molten

PCL in the syringe barrel using a motor that drives the spool core. The co-axial fiber is then released from the bottom of the syringe and cooled down during the transport to the spool core, where it is wound for use in the printing process. The diameter of the filament depends on: (1) the diameter of the fiber threads; (2) the inner diameter of the extrusion needle; and (3) the speed at which the filament is being pulled. For each needle diameter, there is a range of optimum motor rotational speeds that ensure consistent polymer coating; high speeds lead to thin and uneven polymer coatings, while slow speeds result in the formation of polymer beads along the filament.

For the co-axial fiber fabrication setup in fig. 1, the diameter of the fiber threads is  $\sim 0.4\text{mm}$ , the extrusion needle inner diameter is  $1\text{mm}$ , and the filament is being pulled at a speed of  $\sim 0.9\text{mm/s}$ . The resultant co-axial fiber has a diameter of  $\sim 0.9\text{mm}$ . To improve the printed device resolution, the co-axial fiber diameter can be modified by reducing the number of fiber threads within the filament, or decreasing the inner diameter of the extrusion needle. Co-axial fiber diameters that are feasible using the materials demonstrated in this paper range from  $0.4\text{mm}$  to  $1.2\text{mm}$ .

### **Printhead Design**

A major consideration in our printhead design focuses on the development of a long, slender profile to enable 3D printing along highly articulating profiles. The design consists of three main sub-systems: (1) an actuation system, (2) an anchoring system, and (3) an extraction system. Each sub-system is driven with a stepper motor. Unlike common FDM printhead designs that incorporate a motor at the printing tip, a slender profile requires additional mechanisms to transfer the motor action to the printing tip.

#### **A. Actuation system**

The actuation system consists of a driving motor with gripping wheels, a long metal tube that directs the co-axial fiber to the extraction system, and a nozzle that deposits the co-axial fiber filament onto the printing surface (see fig. 2). The driving motor is a NEMA 17 motor with a convention FDM gripper wheel. A gripper wheel with a rubber outer lining provides a flexible surface for effectively directing the co-axial fiber.

The two gripping wheels rotate as the motor turns, sending the polymer coated filament into the long metal tube. The metal tube is  $\sim 150\text{mm}$  long with an inner diameter of  $2\text{mm}$ . The tube deposits the co-axial fiber directly below the extractor (cutting blade) that is elevated until actuated. The polymer coating of our co-axial fiber enables the fiber to traverse the  $150\text{mm}$  long tube without becoming tangled or buckling, which is a common occurrence with uncoated carbon fiber bundles.

The co-axial fiber enters a bent nozzle after exiting the alignment tube. The role of this nozzle is to bend the filament with a  $\sim 5\text{mm}$  radius, therefore allowing the filament to be deposited tangentially to the substrate rather than in a perpendicular orientation. This reduces clogging and

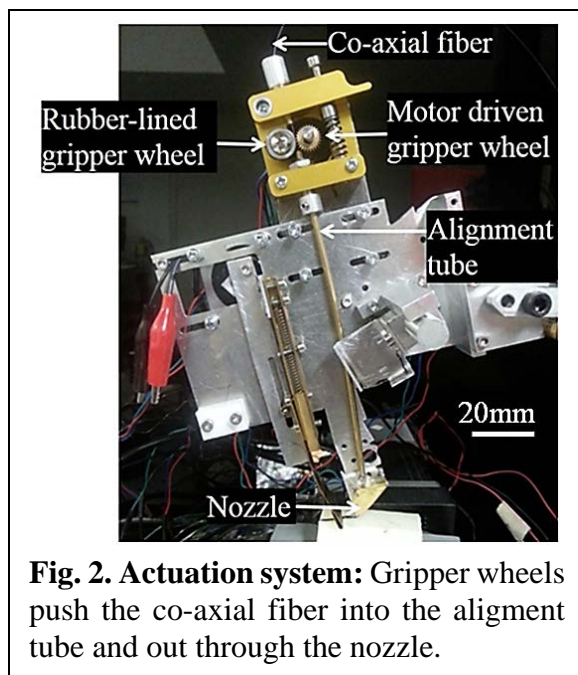


**Fig. 2. Actuation system:** Gripper wheels push the co-axial fiber into the alignment tube and out through the nozzle.

misalignment issues that occur due to the sudden change in direction from perpendicular to tangential when the co-axial fiber is deposited using a vertical orientation.

### B. Filament anchoring system

The filament anchoring system is comprised of a motor (NEMA 17), crank shaft, and heating pad (see fig. 3). As the motor turns, the crank shaft (pivoted in the middle) will transfer the rotational motion of the motor shaft to the heating pad. The heating pad is heated with loops of copper wires charged with a 5V DC supply, and can move in both clockwise and counter-clockwise directions. The heating pad supplies a small thermal source to heat the polymer coating of the co-axial fiber, and enable the fiber to adhere to the substrate surface. The rotational movement from the crankshaft combined with the compression from the springs and flexible heating pad allows the printhead to deform elastically as required by the substrate geometry.

A major challenge in the filament anchoring system stems from the adhesion challenges with the co-axial fiber filament. When the polymer coating of the co-axial filament melts, the molten polymer coating becomes an adhesive agent. As the temperature of the filament decreases, the adhesive nature of the molten polymer reduces. As one might expect, the molten polymer has a stronger adhesion to the higher temperature heating element as compared to the substrate. To minimize the adhesion forces between the polymer and the heating pad, a rocking motion has been introduced with the crankshaft, enabling the heating pad to transfer the co-axial fiber to the substrate.

It is important to note that the heating element in our design is not attached to the nozzle, a common design approach in many FDM printing systems. This separation between the heating element and the nozzle is critical to ensure that the polymer coating of the co-axial fiber filament does not melt within the nozzle and cause the system to clog.

### C. Extraction system

The extraction system contains a NEMA 17 motor with a 5:1 gear-box, a rotational-to-linear motion conversion mechanism and a pivoted cutting blade (fig. 4). The gear-box provides a torque multiplier to drive the cutting blade with a strong force. The rotational-to-linear motion conversion mechanism also provides a multiplier to the force generated by the motor. The cutting blade is modeled after a nail cutter (fig. 4) with a pivot screw localizing cutting force along the blade.

To initiate the extraction process, the motor drives the cutting blade onto the co-axial fiber,

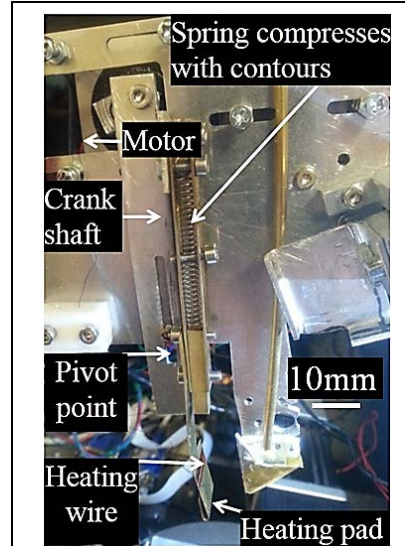


**Fig. 3. Filament anchoring system:** A cyclical motion aids in compression and adherence of the co-axial fiber onto the substrate.

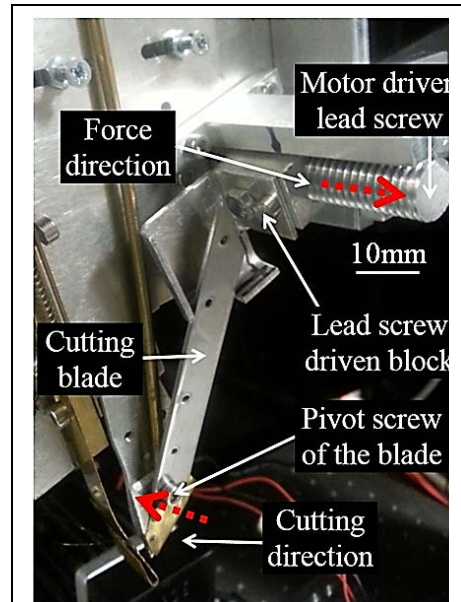


**Fig. 4. Extraction system:** A lead screw converts rotational motion into linear motion to provide the cutting force.

severing the filament along the blade. Once the co-axial filament has been severed, the driving motor from the actuation system recoils the co-axial cable to ensure a clear separation between the two severed ends. In the last step, the cutting blade is retracted into a raised position while the co-axial fiber returns to the tip of the nozzle, thereby resetting the extraction system.

Importantly, the extraction system must be activated approximately 10mm prior to the desired location. The delay is a function of the separation between the extraction location and the printing tip. The remaining co-axial fiber is passively deposited by the anchored filament onto the printing surface.

#### D. Printer setup

Figure 5 provides an image of the FRP system located in the authors' lab. The 4-degrees of freedom (4-DOF) system consists of Aerotech X, Y, Z and rotary motor stages with an XY resolution of 1 micron, Z resolution of 2 $\mu$ m, and rotatory stage with a 1-degree resolution. The printhead is mounted to the Z-axis stage, while the substrate is mounted to the rotatory stage mounted on the XY stage. The printhead has been designed to handle tilted surfaces in the YZ plane up to 65° in the positive and negative direction from the horizontal. Although the current design can only follow contours in the YZ plane, future designs will enable arbitrary contour following. The combined motion of the 4 stages enables the printhead to deposit complicated 3D patterns of co-axial fibers on the printing surface.

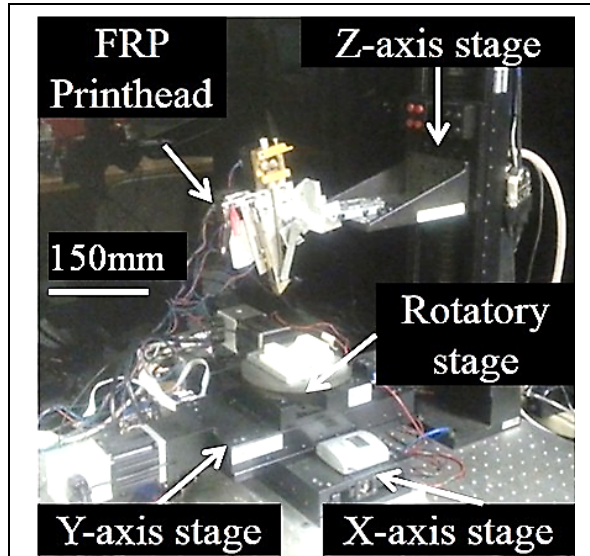


Fig. 5. Custom FRP printer with 4-DOF

#### Printing Demonstrations

To demonstrate the complex deposition capabilities of this FRP printer and highlight geometries that cannot be printed with current fiber reinforced polymer printers, this section presents three parts printed on Polyvinyl Alcohol (PVA) support substrates. PVA was selected as the substrate / support structure material due to its ability to be dissolved in water, and thus separated easily from the printed FRP structure.

##### A. Bi-planar printing

A CAD drawing of a bi-planar (YZ, XY) PVA support substrate and co-axial fiber deposition path is provided in fig. 6.

The outer, bi-planar lines (red lines in fig. 6) are printed first followed by the more conventional, rastered lines along the contoured (YZ) surface (black lines in fig. 6). While either of the planes could be oriented to enable conventional FRP printers to fabricate the lines, the combined pattern

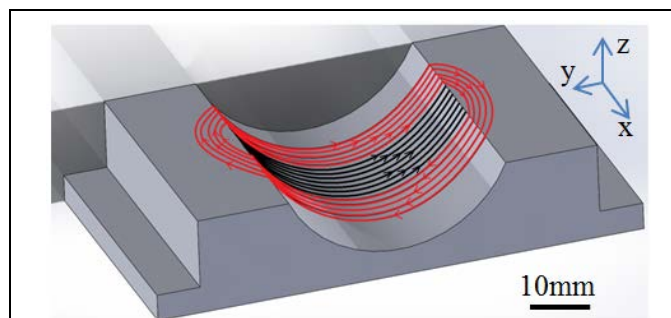
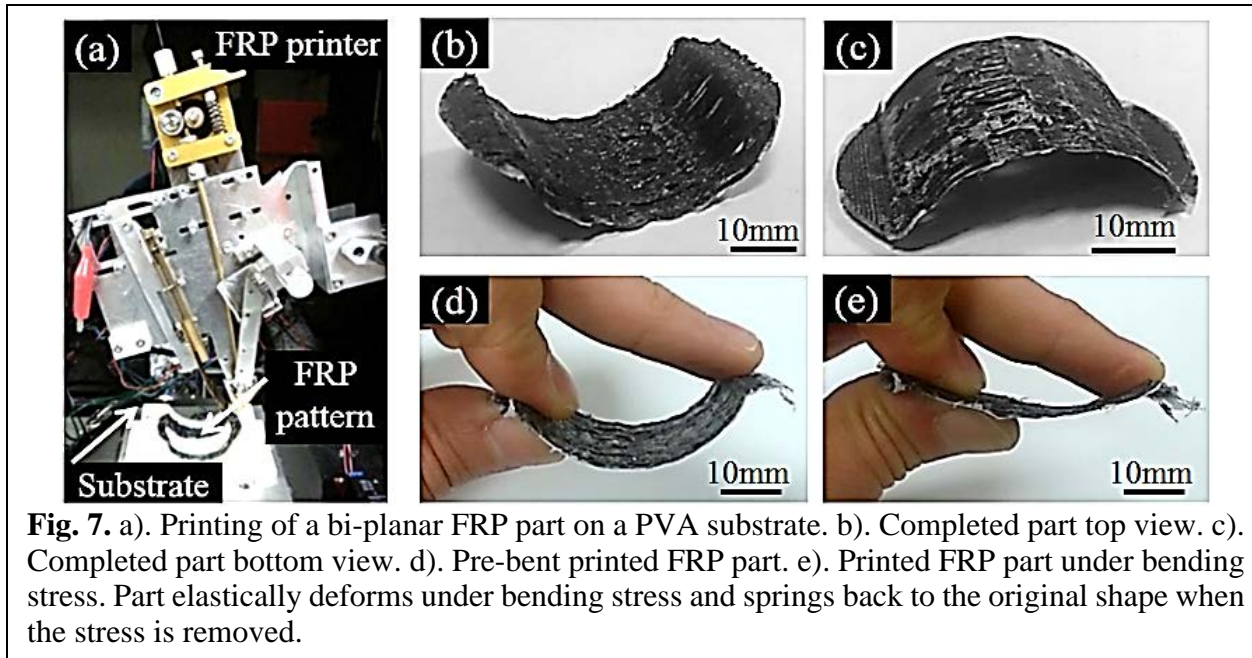
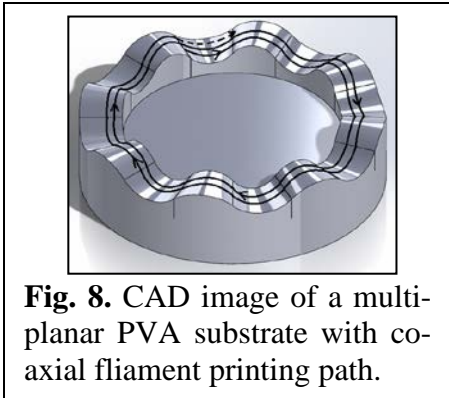


Fig. 6. CAD drawing of the bi-planar PVA substrate and desired co-axial filament printing path. Curved loops (red lines) were followed by repetitive rasters (black lines).

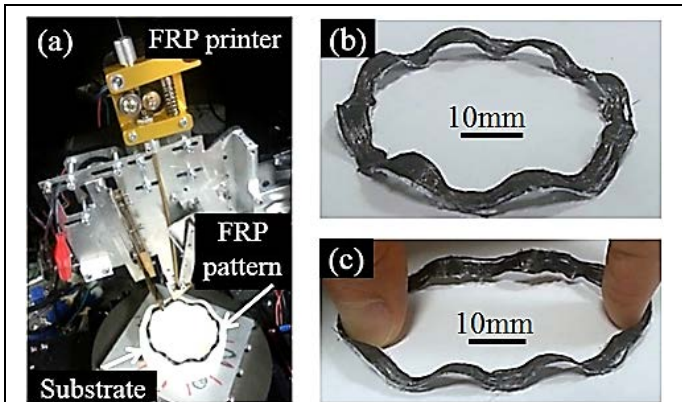


contains seamless transitions between the planes, thereby requiring printing along a contoured surface. This pattern represents the first demonstration of contoured, 3D FRP printing. Figure 7a shows the FRP printing in progress, while figs. 7b and 7c show the completed part after it has been removed from the PVA substrate base. Single layer co-axial fiber patterns (0.9 mm diameter lines, 1 mm layer thickness) were found to be flexible and easily extracted from the PVA substrate base. Importantly, the mechanical behavior demonstrated in fig. 7e follows that of FRP components fabricated using conventional manufacturing methods as compared to FRP components fabricated on FDM-style printers.



### B. Multi-planar printing

Figure 8 shows a CAD drawing of a multi-planar PVA support substrate and the path of the co-axial fiber. Eight loops of co-axial fiber were printed on the multi-planar support substrate. Figure 9a shows the FRP printing in progress, while fig. 9b shows the completed FRP pattern after it has been removed from the multi-planar PVA substrate base.



The design in fig. 8 consists of repeating curves in the YZ, XZ and XY planes. This particular architecture was chosen as it represents a simple design that cannot currently be fabricated using existing FRP printing systems. Similar to the elastic deformation demonstrated with the bi-planar part, fig. 9c illustrates the deformation capabilities of the multi-planar part.

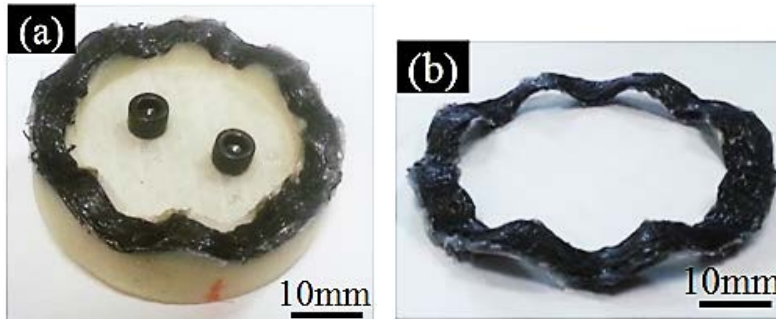


**Fig. 10.** a). Multi-layered, multi-planar FRP printed pattern on PVA substrate. b). Multi-layered, multi-planar printed part after being removed from the PVA substrate. The five layers enhance structural strength and decrease elastic deformation.

### C. Multi-layered, multi-planar printing

Utilizing the substrate architecture from fig. 8, this section demonstrates a multi-layered, multi-planar printed 3D-FRP pattern. Each of the five layers consists of 8 curved loops (~60 mm diameter), with the layers deposited in an overlapping fashion. To ensure adhesion between the layers, the co-axial fibers were pressed into the previously deposited layer. This resulted in layers that were slightly smaller than the single layered pattern (~2.7 mm across 5 layers). The printed part on the PVA supporting substrate is shown in fig. 10a. The addition of multiple layers resulted in a much stronger adhesive force between the substrate and the printed pattern, requiring the substrate to be dissolved in water to retrieve the printed FRP pattern (fig. 10b). Additionally, the extra layers significantly decreased the elastic deformation characteristics of the printed pattern.

### Discussion

The experimental results presented in figs. 7, 9 and 10 provide the first demonstration of contoured, multi-layered *additively manufactured* FRP parts. While the fabrication of contoured, multi-layered FRP parts has been demonstrated using conventional methods such as stacking layers of FRP sheets within a mold, the ability to achieve real-time design customization through additive manufacturing presents a unique capability that will expand the application of FRP in commercial technologies.

One of the most important innovations of our FRP printing system stems from the use of a co-axial fiber that enables fiber deposition in 3-dimensions (XYZ planes) within the same build. The co-axial cables provides the structural support necessary to guide and adhere fibers out of the XY plane; existing FRP 3D printers can only deposit fibers in the XY plane. This additional functionality enables contoured and 3-dimensional FRP printing for the first time. The impact of this advancement will be two-fold: (1) Customized 3D printing of contoured FRP components will enable the use of FRPs in applications ranging from the automotive and aerospace industries to the biomedical field. (2) The co-axial fiber provides a unique structural support mechanism that can be leveraged during the fabrication process to customize the strength-to-weight ratio, and provide previously unattainable 3D printed design features such as overhanging features, contoured shell structures, and 3-dimensional shapes.

Despite the success of this initial prototype, there are important design modifications that will further enhance the fabrication capabilities of our FRP printing system. For example, a more compact printhead design across all subsystems will enable the fabrication of higher resolution patterns within a broader design space (e.g. right-angles, 360 degree continuous depositions).

Additionally, to extend 3D printing of contoured FRP patterns to commercial applications will require a faster, more flexible, cost effective, and robust printing system. Future FRP printing system designs aim to address this need.

### **Conclusion**

The use of fiber reinforced polymer materials has been growing within the automotive, aerospace and biomedical industries, driving the development of corresponding 3D printing technologies. Currently FRP printing techniques are unable to align fibers along a contoured surface, therefore preventing them from creating shell structures with similar strength-to-weight ratios as those made with traditional layering/mold approaches. The FRP printing system detailed in this manuscript provides the first demonstration of 3D printed FRP patterns with the fibers aligned along the contour profile. This represents a significant step towards customized 3D printing of functional contoured structures. Additionally, advancements in the printhead design will address the need for a faster, more flexible and robust printing system. Finally, we will scale up the printing system to extend the applications to the automotive and aerospace industries.

### **References**

- [1] K. V. Wong, and A. Hernandez, "A review of additive manufacturing," *ISRN Mechanical Engineering*, 2012.
- [2] S. H. Huang, P. Liu, A. Mokasdar, and L. Hou, "Additive manufacturing and its societal impact: a literature review," *Int J Adv Manuf Tech*, 67(5-8), pp. 1191-1203, Jul. 2013.
- [3] W. E. Frazier, "Metal additive manufacturing: a review," *J Mater Eng Perform*, 23(6), pp. 1917-1928, Jul. 2014.
- [4] I. Gibson, D. Rosen and B. Stucker, "Additive manufacturing technologies: 3D printing, rapid prototyping, and direct digital manufacturing," Springer, 2014. ch. 3, sec. 7.5, pp. 10, 57
- [5] S. H. Ahn, H. J. Lee and G. H. Kim, "Polycaprolactone scaffolds fabricated with an advanced electrohydrodynamic direct-printing method for bone tissue regeneration," *Biomacromolecules*, vol. 12, no. 12, pp. 4256-4263, Nov. 2011.
- [6] S. Das, S. J. Hollister, C. Flanagan, A. Adewunmi, K. Bark, C. Chen, K. Ramaswamy, D. Rose and E. Widjaja, "Freeform fabrication of Nylon-6 tissue engineering scaffolds," *Rapid Prototyping J*, vol. 9, no. 1, pp.43-49, Mar. 2003.
- [7] P. Liacouras, J. Garnes, N. Roman, A. Petrich and G. T. Grant, "Designing and manufacturing an auricular prosthesis using computed tomography, 3-dimensional photographic imaging, and additive manufacturing: a clinical report," *J Prosthet Dent*, vol. 105, no. 2, pp. 78-82, Feb. 2011.
- [8] A. Grzesiak, R. Becker and A. Verl, "The bionic handling assistant: a success story of additive manufacturing," *Assembly Autom*, vol. 31, no. 4, pp. 329-333, Sep. 2011.
- [9] D. Hull and T. W. Clyne, "An introduction to composite materials," Cambridge University Press, 1996, pp.4
- [10] B. G. Compton and J. A. Lewis, "3D-printing of lightweight cellular composites," *Adv Mater*, vol. 26, no. 34, pp. 5930-5935, Sep. 2014.
- [11] U.S. Environmental Protection Agency. (2012, August). *EPA and NHTSA Set Standards to Reduce Greenhouse Gases and Improve Fuel Economy for Model Years 2017-2025 Cars*

- and Light Trucks*. [Online]. Available: <http://www.epa.gov/otaq/climate/documents/420f12051.pdf>.
- [12] Dept of Transportation. (2013 April) *National Highway Traffic Safety Administration, Federal Register Volume 78, Number 66, 49 CFR Part 575*. [Online]. Available: <http://www.gpo.gov/fdsys/pkg/FR-2013-04-05/html/2013-07766.htm>;
- [13] L. M. Sherman.(2007 September). *Plastics Technology. What's New at the Show In PUR/RIM* [Online]. Available: <http://www.ptonline.com/articles/what's-new-at-the-show-in-pur-rim>
- [14] A. Brecher, J. Brewer, S. Summers and S. Patel, “Characterizing and Enhancing the Safety of Future Plastic and Composite Intensive Vehicles (PCIVs)” in *The 21<sup>st</sup> International Technical Conference on the Enhanced Safety of Vehicles*, 2009 [Online]. Available: <http://www-nrd.nhtsa.dot.gov/pdf/esv/esv21/09-0316.pdf>.
- [15] D. Sedgwick. (2011 July) *Automotive News. New techniques cut cost of carbon fiber* [Online]. Available: <http://www.autonews.com/article/20110711/OEM01/307119988/new-techniques-cut-cost-of-carbon-fiber>
- [16] T. Dunne. (2013 April) J.D. Power Global Auto Blog. *One-Third of Vehicle Mix to Feature Alternative Powertrains in 2025*. [Online]. Available: <http://www.jdpowercontent.com/globalauto/one-third-of-vehicle-mix-to-feature-alternative-powertrains-in-2025/2013/04/29/>.
- [17] International Committee of the Red Cross’s Physical Rehabilitation Programme, “Knee-Ankle-Foot Orthosis: Manufacturing Guidelines,” 2006.
- [18] S. J. Lochner, J. P. Huissoon, and S. S. Bedi, “Simulation Methods in the Foot Orthosis Development Process,” *Comput. Aided. Des. Appl.*, vol. 11, no. 6, pp. 608–616, Jun. 2014.
- [19] M. C. Faustini, R. R. Neptune, R. H. Crawford, and S. J. Stanhope, “Manufacture of Passive Dynamic Ankle–Foot Orthoses Using Selective Laser Sintering,” *IEEE Trans. Biomed. Eng.*, vol. 55, no. 2, pp. 784–790, Feb. 2008.
- [20] C. Mavroidis, R. G. Ranky, M. L. Sivak, B. L. Patritti, J. DiPisa, A. Caddle, K. Gilhooly, L. Govoni, S. Sivak, M. Lancia, R. Drillio, and P. Bonato, “Patient specific ankle-foot orthoses using rapid prototyping.,” *J. Neuroeng. Rehabil.*, vol. 8, no. 1, pp. 1, Jan. 2011.
- [21] J. A. Owusu, and K. Boahene, “Update of patient-specific maxillofacial implant.,” *Curr Opin Otolaryngol Head Neck Surg*, Vol. 23, no. 4, pp. 261-4, Aug. 2015
- [22] A. L. Jardini, M. A. Larosa, R., Maciel Filho, C. A. de Carvalho Zavaglia, L.F. Bernardes, C. S. Lambert, D. R. Calderoni and P. Kharmandayan, “Cranial reconstruction: 3D biomodel and custom-built implant created using additive manufacturing”. *J Craniomaxillofac Surg*, vol.42, no. 8, pp. 1877-84, Dec. 2014
- [23] K. C. Wong, S. M. Kumta, N. V. Geel, and J. Demol, “One-step reconstruction with a 3D-printed, biomechanically evaluated custom implant after complex pelvic tumor resection”. *Comput Aided Surg*, vol. 20, no. 1, pp. 14-23, Jan.2015
- [24] J. Chen, Z. Zhang, X. Chen, C. Zhang, G. Zhang, and Z. Xu, “Design and manufacture of customized dental implants by using reverse engineering and selective laser melting technology”. *J Prosthet Dent*, vol. 112, no. 5, pp. 1088-95, Nov. 2014.
- [25] G. Gagg, E. Ghassemieh, and F.E. Wiria, ‘Effects of sintering temperature on morphology and mechanical characteristics of 3D printed porous titanium used as dental implant’. *Mater Sci Eng C Mater Biol Appl*, vol. 33, no. 7, pp. 3858-64, Oct. 2013

- [26] N. Xu, F. Wei, X. Liu, L. Jiang, H. Cai, Z. Li, M. Yu, F. Wu, and Z. Liu, "Reconstruction of the Upper Cervical Spine Using a Personalized 3D-Printed Vertebral Body in an Adolescent With Ewing Sarcoma". *Spine*, vol. 41, no. 1, pp. E50-4, Jan. 2016
- [27] N. E. Fedorovich, W. Schuurman, H. M. Wijnberg, H. J. Prins, P. R. van Weeren, J. Malda, J. Alblas, and W. J. Dhert, "Biofabrication of osteochondral tissue equivalents by printing topologically defined, cell-laden hydrogel scaffolds". *Tissue Eng Part C Methods*, vol. 18, no. 1, pp. 33-44, Sep. 2012.
- [28] C. G. Jeong, and A. Atala, "3D Printing and Biofabrication for Load Bearing Tissue Engineering". in *Engineering Mineralized and Load Bearing Tissues vol. 881* Switzerland, Springer International , 2015. pp. 3-14.
- [29] T. Xu, K. W. Binder, M.Z. Albanna, D. Dice, W. Zhao, J. J. Yoo, and A. Atala, "Hybrid printing of mechanically and biologically improved constructs for cartilage tissue engineering applications". *Biofabrication*, vol 5, no. 1, pp. 015001, Nov. 2013
- [30] F. Obregon, C. Vaquette, S. Ivanovski, D. W. Hutmacher, and L. E. Bertassoni, "Three-Dimensional Bioprinting for Regenerative Dentistry and Craniofacial Tissue Engineering". *J Dent Res*, 94(9 Suppl), pp. 143S-52S, Jun. 2015.
- [31] J. H. Park, J. M. Hong, Y. M. Ju, J. W. Jung, H. W. Kang, S. J. Lee, J. J. Yoo, S. W. Kim, S. H. Kim, and D. W. Cho, "A novel tissue-engineered trachea with a mechanical behavior similar to native trachea". *Biomaterials*, vol. 62, pp. 106-15, Sep. 2015.
- [32] J. Visser, F. P. Melchels, J. E. Jeon, E. M. van Bussel, L. S. Kimpton, H. M. Byrne, W. J. Dhert, P. D. Dalton, D. W. Hutmacher, and J. Malda, "Reinforcement of hydrogels using three-dimensionally printed microfibers". *Nat. Commun.*, vol. 6, pp. 6933, Apr. 2015.